A new family of borated glasses as a corrosion inhibitor for steel in 1.0 M hydrochloric acid: synthesis and cauterization studies

A. Elbadaoui,[1] M. Galai,[2]* S. Ferraa,[1] H. Barebita,[1] M. Cherkaoui[1,3] and T. Guedira[1]

[1]Laboratory of Organic, Inorganic Chemistry, Electrochemistry and Environment, Faculty of Sciences, Ibn Tofaïl University, PO Box 133, 14000, Kenitra, Morocco
[2]Advanced Materials and Process Engineering, Faculty of Sciences, Ibn Tofaïl University, PO Box 133, 14000, Kenitra, Morocco
[3]National Higher School of Chemistry (NHSC), University Ibn Tofail BP. 133-14000, Kenitra, Morocco
**E-mail: galaimouhsine@gmail.com*

Abstract

The influence of $(0.90-x)Bi_2O_3-xB_2O_3-(0.05V_2O_5-0.05Nb_2O_5)$ on the corrosion of mild steel in 1 M HCl was investigated. Electrochemical polarization and impedance spectroscopic studies were used. The submerged surface of steel was studied by scanning electron microscopy coupled with Energy Dispersive X-Ray Spectroscopy (SEM/EDS). The inhibition efficiency increases with B_2O_3 content to reach 92% at 150 ppm. Polarization curves show that NA1 acts as an anodic inhibitor. The inhibition efficiency increases with increasing inhibitor concentration to 98.6% at 150 ppm. On the other hand, electrochemical impedance data show that addition of the 150 ppm NA1 decreases the double layer capacitance and simultaneously increases the charge transfer resistance of the corrosion process. The effect of temperature on the corrosion behavior of mild steel in 1 M HCl without and with addition of 150 ppm NA1 was studied in the temperature range from 298 to 328 K. An increase in temperature leads to a decrease in the inhibition efficiency of both inhibitors. A thermodynamic study showed that the film was formed due to physisorption in the presence of an inhibitor. Scanning electron microscopy (SEM) confirms the performance of our inhibitors against corrosion. Moreover, the results of this study showed that the inhibition efficiencies depend to the B_2O_3, V_2O_5 and Nb_2O_5 content in the system.

Received: July 4, 2021. Published: May 11, 2022 doi: 10.17675/2305-6894-2022-11-2-15

Keywords: *acid corrosion, glass, surface analysis, polarization, inhibition.*

1. Introduction

Acid solutions are commonly used for the removal of undesirable scale and rust at metallurgic works, in the cleaning of boilers and heat exchangers. Hydrochloric acid is most widely used for all these purposes. However, over-pickling of metal leads to a rough, blistered surface. The formation of a protective film on steel surface and characterization of

metal surface are the major subjects of interest. Carbon steel is among the most widely used engineering materials such as metal-processing equipment, marine applications, nuclear and fossil fuel power plants, transportation, chemical processing, pipelines, mining and construction. Iron and its alloys as construction materials in industrial sectors have become a great challenge for corrosion engineers and scientists nowadays [1]. In order to reduce the corrosion rate of metals, several techniques have been applied. The use of inhibitors is one of the most practical methods for protection against corrosion in acidic media. Inhibitors that reduce the corrosion of metallic materials can be divided into three kinds: surfactant inhibitors [2], organic inhibitors [3] and inorganic inhibitors [4]. Heterocyclic inhibitors have many advantages such as high inhibition efficiency [5–8], low price, and easy production.

The choice of effective inhibitors is based on their mechanism of action and their electron- donating capability. Moreover, inhibitory ability is reinforced by the presence of a molecular structure with adsorption active sites comprising lone electron pairs and/or π-orbitals, such as heterocyclic rings containing sulphur, oxygen, phosphorus and/or nitrogen atoms [9–11]. These compounds can form either a strong coordination bond with metal atom or a passive film on the surface [12]. The corrosion inhibition of a metal may involve either physisorption or chemisorption of the inhibitor on the metal surface. Electrostatic attraction between the charged hydrophilic groups and the charged active centers on the metal surface leads to physisorption. Several authors showed that most inhibitors were adsorbed on the metal surface by displacing water molecules from the surface and forming a compact barrier film [13]. The choice of an optimal inhibitor should be based on three considerations: (I) convenient synthesis from inexpensive raw materials, (II) the presence of phosphorus, nitrogen, oxygen, sulfur and multiple bonds in the inhibitor molecule are required for its efficiency and (III) its toxicity toward the environment must be negligible [14].

The purpose of this paper is aimed to study the axis NA as a corrosion inhibitor of mild steel in 1 M HCl solution at 298 K using weight loss, electrochemical impedance spectroscopy (EIS) and potentiodynamic polarization measurements.

2. Experimental Part

Various vitreous samples were synthesized from vanadium oxide V_2O_5 (Aldrich), bismuth oxide Bi_2O_3 (Aldrich), boron oxide B_2O_3 (Aldrich), and niobium oxide Nb_2O_5 (Fluka). The vitreous compositions of the system $Bi_2O_3–B_2O_3–(0.5Nb_2O_5–0.5V_2O_5)$ were made by stoichiometric mixing of the raw materials according to the reaction scheme:

$$\left(1-x-y\right)\mathrm{Bi_2O_3}+x\mathrm{B_2O_3}+\frac{y}{2}\mathrm{Nb_2O_5}+\frac{y}{2}\mathrm{V_2O_5}\xrightarrow{\boldsymbol{T}}\left(1-x-y\right)\mathrm{Bi_2O_3}-x\mathrm{B_2O_3}-\frac{y}{2}\mathrm{Nb_2O_5}-\frac{y}{2}\mathrm{V_2O_5}$$

where ***T*** signifies thermal treatment.

The mixtures were crushed in an agate mortar. The thermal operation was conducted in alumina crucibles. The first treatment at 350°C for 15 hours allows the removal of hydrogen; it was followed by homogenizing grinding. Each reaction mixture was then heated to 1050°C, *i.e.*, above the melting temperature, and then dipped energetically into an alumina

mold preheated to 200°C. The infrared spectra ware recorded between 4000 and 400 cm^{-1} using a Perkin Elmer1600 Fourier transform spectrometer. For the XRD study, we used an X'Pert^3 Powder instrument from Malvern Panalytical; the radiation was $\lambda_{K\alpha}$(Cu)=1.5406 Å.

The experiments were performed with mild steel (MS) with the chemical composition (in wt%) presented in Table 1.

Table 1. The chemical composition of mild steel (MS).

C	Si	Mn	Cr	Mo	Ni	Al	Cu	Co	V	W	Fe
0.11	0.24	0.47	0.12	0.02	0.1	0.03	0.14	<0.0012	<0.003	0.06	Balance

The aggressive solutions of 1.0 M HCl were prepared by dilution of concentrated 37% HCl with an appropriate amount of distilled water.

The working electrodes were abraded with emery paper (up to 1200 grit), cleaned with acetone and washed with distillated water, and finally dried at hot air before being immersed in the acid solution. The concentrations of inhibitor were varied from 100 to 300 ppm.

2.1. Electrochemical measurements

Electrochemical experiments were carried out using a PGZ100 potentiostat/galvanostat in a conventional three-electrode cell with a platinum counter electrode (CE) and a saturated calomel electrode (SCE) as a reference electrode. All potentials were given with respect to it. The electrodes were carefully positioned in the cell for reproducible geometry. In addition, the working electrode was immersed in the test solution for half an hour until a steady state open circuit potential (E_{ocp}) was obtained. All electrochemical experiments were conducted at 298±2 K using 50 ml of the test solution.

Tafel polarization curves were recorded by scanning the electrode potential from –900 mV/SCE to –100 mV/SCE at a scanning rate of 1 mV/s. To evaluate corrosion kinetic parameters, fitting by the Stern–Geary equation was used. To do so, the overall current density values, *i*, were considered as the sum of two contributions, anodic and cathodic currents i_a and i_c, respectively. For the potential domain not too far from the open circuit potential, it may be considered that both processes followed the Tafel law [15]. Thus, it can be derived from equation (1):

$$i = i_a + i_c = i_{corr}\{\exp[b_a \cdot (E - E_{corr})] - \exp[b_c \cdot (E - E_{corr})]\} \quad (1)$$

where i_{corr} is the corrosion current density ($A \cdot cm^{-2}$), b_a and b_c are the Tafel constants of anodic and cathodic reactions (V^{-1}), respectively. These constants are linked to the Tafel slopes β (V/dec) in the usual logarithmic scale given by equation (2):

$$\beta = \frac{\ln 10}{b} = \frac{2.303}{b} \quad (2)$$

The corrosion parameters were then evaluated by means of nonlinear least squares method by applying equation (2) using Origin software. However, for this calculation, the

potential range applied was limited to ±0.100 V/SCE around E_{corr}, else a significant systematic divergence was sometimes observed for both anodic and cathodic branches.

The corrosion inhibition efficiency was evaluated from the corrosion current density values using the relationship (3):

$$\eta_{pp} = \frac{i_{corr}^0 - i_{corr}}{i_{corr}^0} \cdot 100 \quad (3)$$

where i_{corr}^0 and i_{corr} are the corrosion current density values without and with an inhibitor, respectively.

Electrochemical impedance spectroscopy measurements were carried out using a transfer function analyzer (VoltaLab PGZ 100), with a small amplitude a.c. signal (10 mV rms), over a frequency domain from 100 kHz to 100 mHz with five points per decade. The EIS diagrams were plotted in the Nyquist representation. The results were then analyzed in terms of an equivalent electrical circuit using the Bouckamp's program [16].

The inhibiting efficiency derived from EIS, η_{EIS}, was calculated using the following equation (4):

$$\eta_{EIS} = \frac{R_{ct} - R_{ct}^0}{R_{ct}} \cdot 100 \quad (4)$$

where R_{ct}^0 and R_{ct} are the charge transfer resistance values in the absence and in the presence of an inhibitor, respectively.

2.2. Surface characterization by SEM/EDX

The nature of the film formed on the surface of the metal exposed to 1.0 M HCl solution for 6 h in the absence and in the presence of the studied inhibitor was determined by Scanning Electron Microscopy (Quanta FEG 450) coupled with EDX analyses. These analyses were performed in foundation MAScIR-Rabat.

3. Results and Discussion

3.1. Delimitation of the vitreous domain

X-Ray diffraction allowed us to identify the vitreous compositions in the studied system. Any sample whose spectrum did not contain diffraction lines is considered as belonging to the vitreous system. Figure 1 shows the defined area and the axis of vitreous systems. This system has already been subject to investigation [17–19].

Tables 2 gives the corresponding molar fractions. Figure 1 shows the X-ray spectra for the EL axis compositions. The X-ray diffraction spectrum from the NA axis is substantially similar.

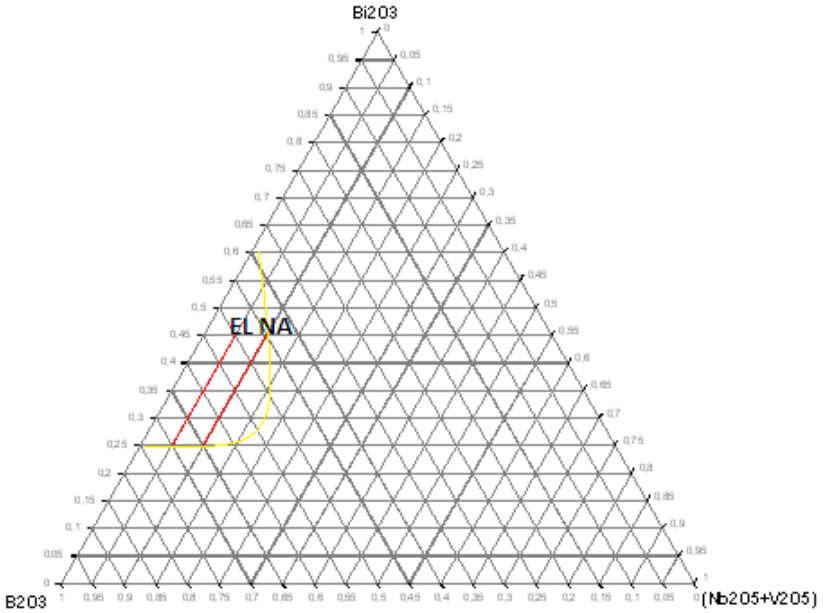

Figure 1. Delimitation of $Bi_2O_3–B_2O_3–[0.5V_2O_5–0.5Nb_2O_5]$ vitreous domainaxe of glassy system was studied: axis (NA): $(0.90–x)Bi_2O_3–xB_2O_3–0.1[V_2O_5–Nb_2O_5]$ with $0.3 \leq x \leq 0.5$.

Table 2. Molar fractions of $(0.90–x)Bi_2O_3–xB_2O_3–(0.05V_2O_5–0.05Nb_2O_5)$.

Sample No.	***x***	**0.90–*x***
NA1	0.3	0.6
NA2	0.35	0.55
NA3	0.4	0.5
NA4	0.45	0.45
NA5	0.5	0.4

3.2. IR study

Figure 2 show the infrared spectra of the (NA) axis. The frequencies and powers are summarized in Table 3.

We notice a widening of the bands. Indeed, in the glassy state, the molecules or groups of atoms are not isolated. These entities are in strong interaction with each other. In a glass sample, a unit cell can be defined and the entire sample must be considered as a single cell containing a giant molecule with an infinite number of entities that vibrate.

From Figure 2, we noticed that the band between 420 cm^{-1} and 490 cm^{-1} covers various structural units. It can be attributed to the B–O–B vibrations [20–22]. The boron atoms in coordination IV are responsible for the appearance of the band between 500 cm^{-1}–540 cm^{-1} and the band at 750 cm^{-1} [23, 24]. The band between 600 cm^{-1}–690 cm^{-1} was assigned to the vibrations of the B–O–P bond in alkaline

borophosphate glasses [25–29]. Scagliotti and NA1 have evoked bands around 1000 cm^{-1} related to O–P–O vibrations which do not appear in our spectrum [30]. The band between 1190 cm^{-1}–1240 cm^{-1} is attributed to the vibration of the B–O^- terminal groups in pyroborate units [31, 32]. The band at 1270 cm^{-1} is attributed to the asymmetric elongation mode of B–O in orthoborate units (BO_3).

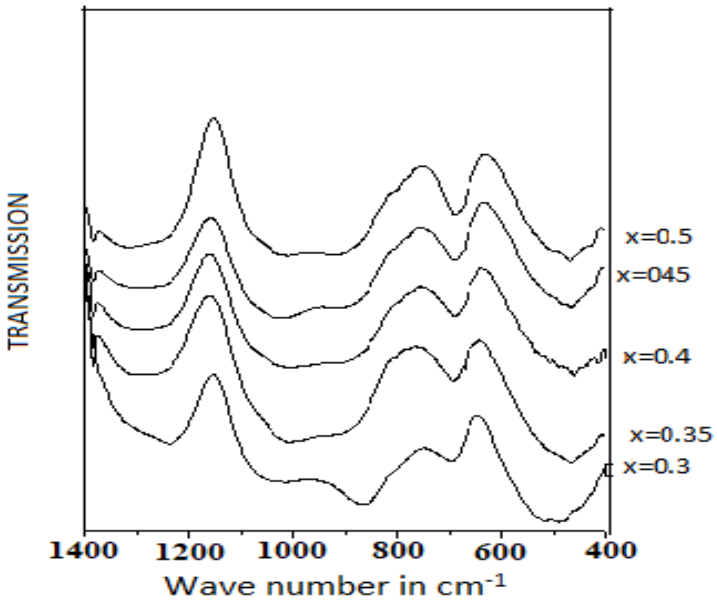

Figure 2. I.R spectra of $(0.90–x)Bi_2O_3–xB_2O_3–0.1[V_2O_5–Nb_2O_5]$.

Table 3. Assignments of IR frequencies for $(0.90–x)Bi_2O_3–xB_2O_3–0.1[V_2O_5–Nb_2O_5]$.

	Sample	NA1	NA2	NA3	NA4	NA5
	Composition	x=0.30	x=0.35	x=0.4	x=0.45	x=0.5
Attributions	–δ Group (B–O–B)	–	–	–	486	466
	or δ (Bi–O–Bi)	475	469	470	–	–
	or δ (Bi–O–B)	507	494	–	–	
	Metaborates υ_s(B–O–Nb)	668	669	–	–	–
	Pyrovanadate group $V_2O_7^{4-}$	777	778	–	–	–
	Group VO_4	798	799	796	–	–
	Metaborate υ_s(B–O–V)	698	701	698	697	693
	Orthovanadate	894	907	910	–	–
	Orthoborate (BO_3)	1032 1008	1030 1008	1028	1030	1033
	Pyroborate B–O–	1235	1310	1311	1324	–
	ν_{as}(BO) in BO_3	1382	1381	1382	1384	1382

As expected, substitution of bismuth by boron leads to an increase in the intensity of the bands assigned to the B–O–Bi and B–O–B groups and a decrease in those associated with Bi–O–B. We also observe an increase in the band intensity attributed to the B–O–P units and a decrease in the band assigned to the pyroborate units. The bands evolution could be attributed to the conversion of the pyroborate units to the metaborate unit. Otherwise, an increase in the Nb_2O_5 and V_2O_5 concentrations results in:

- A decrease in the intensity of the band corresponding to the B–O–P groups.
- Disappearance of the Bi–O–B bands and those assigned to the orthoborate and orthophosphate groups.
- Displacement of the band corresponding to the pyroborates BO^- to higher frequencies.

3.3. Potentiodynamic polarization curves

The potentiodynamic polarization curves obtained from the corrosion behavior of mild steel in 1 M HCl in the absence and in the presence of different concentrations of NA inhibitor at 298 K are shows in Figure 3. Electrochemical corrosion parameters, such as corrosion potential E_{corr} (mV/SCE), cathodic and anodic slopes β_c, β_a, corrosion current density i_{corr}, and inhibition efficiency EI(%) are given in Table 4.

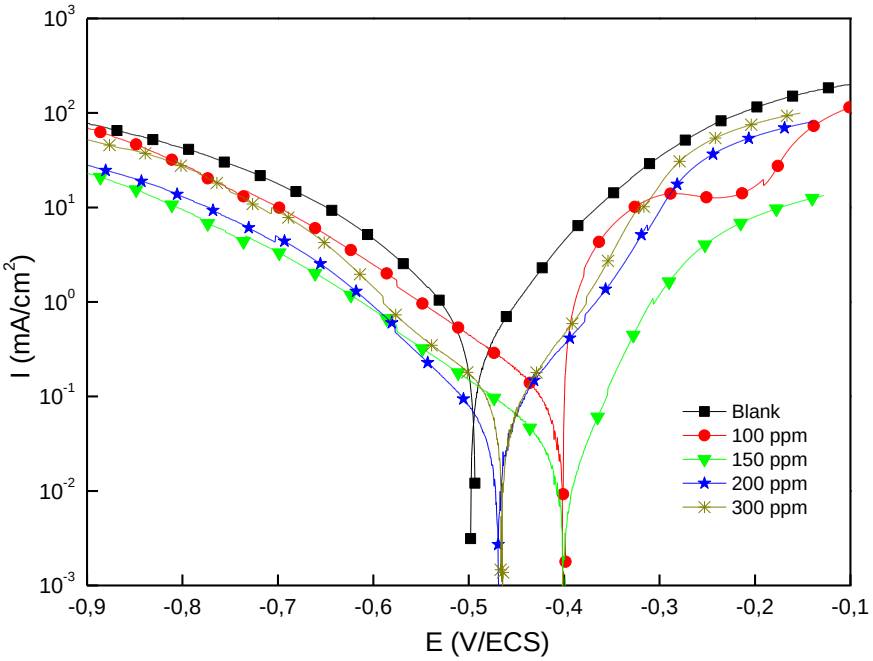

Figure 3. polarization curves for mild steel in HCl with various concentrations of NA1 at 298 K.

It is clear from Figure 3 that addition of NA1 decreases the cathodic and anodic slopes with an increase in inhibitor concentration. As it can be seen from Table 4, when the concentration of the inhibitor increases, the inhibition efficiency increases, while corrosion

current densities increase. Also, we can find that the corrosion potentials shift in the positive direction in HCl solution in the presence of NA inhibitor. According to the literature, if the displacement of E_{corr} with the inhibitor is higher than ±85 mV compared to blank corrosion potential, the inhibitor can be classified as a cathodic or anodic type inhibitor [33]. However, if E_{corr} variation is smaller than ±85 mV, the corrosion inhibitor can be regarded as a mixed-type inhibitor [34]. In the present study, the maximum displacement of E_{corr} is 102 mV, indicating that NA can be classified as an "anodic type inhibitor".

The cathodic curves (Figure 3) give rise to parallel lines indicating that the addition of NA to 1 M HCl solution does not modify the hydrogen evolution mechanism and the reduction of H^+ ions on the mild steel surface which occurs mainly through a charge transfer mechanism.

The inhibitor is first adsorbed on the mild steel surface and blocks the available reaction sites. In this context, the surface area available for H^+ ions decreases while the actual reaction mechanism remains unaffected. These results are confirmed by Guedira [17].

However, the mild steel dissolution rate decreases gradually in the presence of an inhibitor at low anodic over-potentials below −450 mV/SCE and increases sharply. Therefore, it is concluded [18] that the adsorption of the inhibitor molecules on the metal surface gives rise to film formation, which provides good protection for mild steel at low anodic over-potentials. However, this film loses its performance at high anodic potentials. The observed behavior could be explained by significant iron dissolution leading to desorption of the film from the metal surface.

Table 4. Electrochemical parameters of steel at different concentrations of NA1 in 1 M HCl and inhibitory efficiency.

Conc. (ppm)	**$-E_{corr}$ (mV/ECS)**	**i_{corr} (μA/cm²)**	**$-\beta_c$ (mV/dec)**	**β_a (mV/dec)**	***EI*%**	**θ**
Blank	497	983	92	104	–	–
100	395	425	106	96	56.8	0.568
150	397	102	118	43	89.6	0.896
200	464	192	96	76	80.5	0.805
300	461	209	121	68	78.7	0.787

3.4. Electrochemical impedance spectroscopy (EIS)

To understand the corrosion and protection mechanisms that operate on the surface of the metal in the acid medium in the absence and in the presence of NA1 at different concentrations, we recorded electrochemical impedance diagrams at the corrosion potential.

The Nyquist plots of mild steel in 1 M HCl at 298 K in the absence and in the presence of various concentrations of NA1 inhibitor are given in Figure 4. These diagrams were obtained after 1/2 h of immersion in 1 M HCl at 298 K.

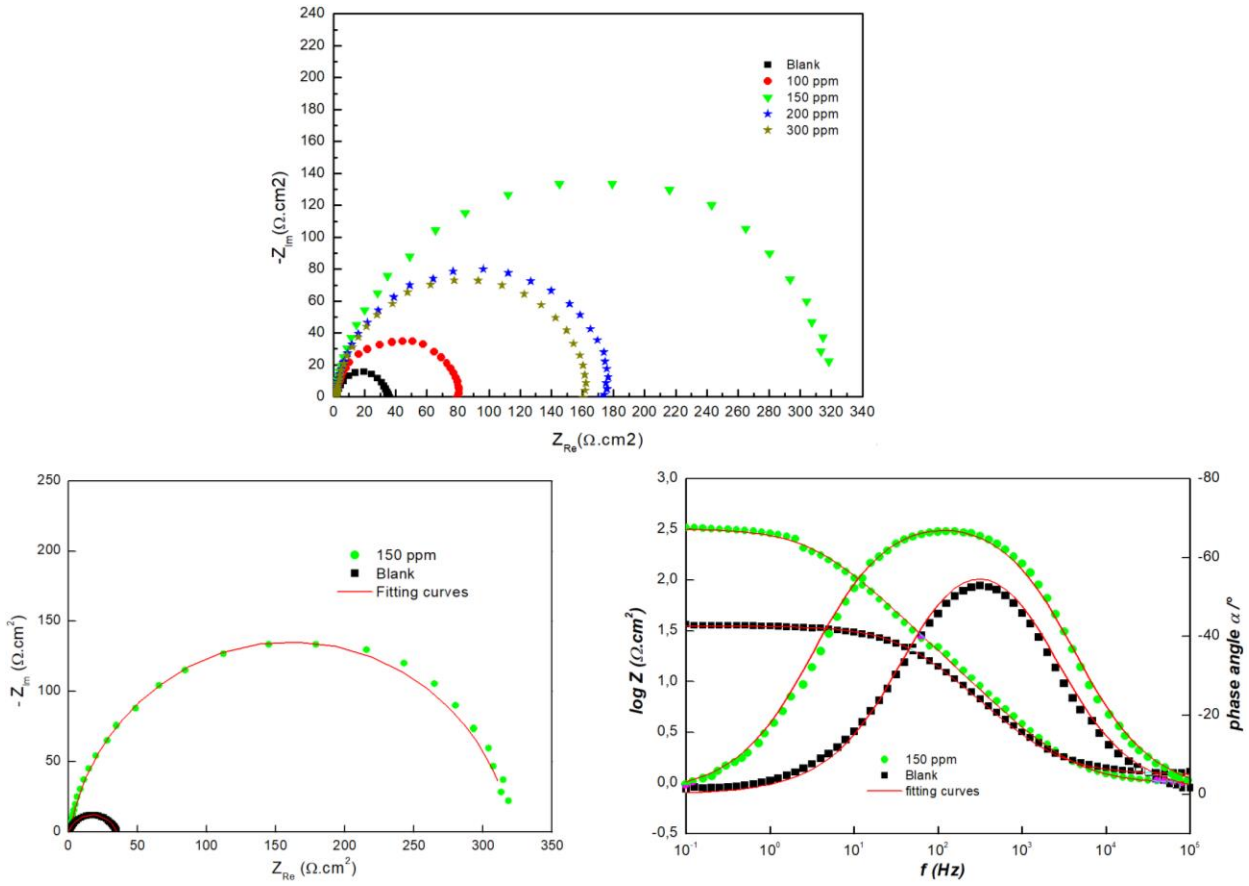

Figure 4. Nyquist and Bode plots of mild steel in 1 M HCl with various concentrations of NA1 at 298 K.

The impedance spectra show that a single semi-circle and the diameter of the semicircle increase in the presence of NA1. The results indicate that NA1 inhibits mild steel corrosion in acid environments. This indicates that the corrosion process of mild steel in 1 M HCl is controlled by the charge transfer phenomenon and addition of NA1 to the electrolytic solution does not change the mechanism of mild steel corrosion in the acid solution [35, 36].

The electrochemical parameters of the corrosion reaction were derived by fitting and simulating the impedance spectra using a simple equivalent circuit of the form shown in Figure 5. This circuit is composed of elements such as a constant phase element (CPE), charge transfer resistance (R_p), and solution resistance (R_s).

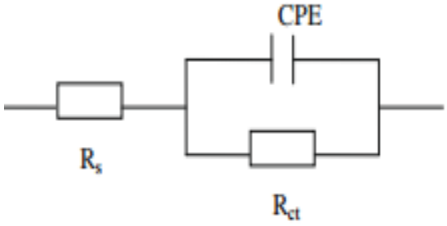

Figure 5. The electrochemical equivalent circuit used to fit the impedance spectra.

CPE was used as the substitute for the capacitor to fit more accurately the impedance behavior of the electric double layer. The impedance of the CPE is expressed as:

$$Z_{\mathrm{CPE}} = Y^{-1}\left(j\omega\right)^{n} \tag{5}$$

where Y is the magnitude of the CPE; ω the angular frequency; n as the deviation parameter ($-1 < n < 1$ which is dependent on the surface morphology). The higher frequency range loops have a depressed semicircular appearance, $0.5 < n < 1$, which is often referred to as frequency dispersion as a result of the non-homogeneity or roughness of the solid surface [37].

The electrochemical parameters of the impedance spectroscopy are given in Table 4. From Table 5 it may be noticed that the R_{ct} value decreases and C_{ct} increases with inhibitor concentration, indicating that more inhibitor molecules are adsorbed on the metal surface and provide better surface coverage and/or enhance the thickness of the protective layer at the metal/solution interface [38]. The inhibition efficiency values increase substantially with an increase in the inhibitor concentration, but the optimum value is 150 ppm indicating that the maximum coverage of the inhibitor on the surface is obtained in a solution with a lower concentration of inhibitors. The impedance study also gave the same efficiency trend as it was found by the Tafel polarization method.

Table 5. Electrochemical parameters of mild steel at different concentrations of NA1 in 1 M HCl and the inhibitory efficiency.

	Conc. (ppm)	R_{ct} **(Ω·cm²)**	C_{dl} **(μF·cm⁻²)**	η_{imp} **%**
1M HCl	–	35	284	–
NA1	100	80	164	56.2
	150	326	58	89.2
	200	176	76	80.0
	300	160	80	78.0

3.5. Effect of temperature

3.5.1. Polarization curves

In order to gain more information about the adsorption type of NA1 and its effectiveness at higher temperatures, potentiodynamic polarization measurements were used in the temperatures range from 298 to 328 K for mild steel electrode in 1 M HCl without and with 150 ppm of NA1 after immersion for 30 min. The results obtained are presented in Figures 6 and 7.

Their corresponding data are collected in Table 6. It is noticed that an increase in solution temperature leads to an increase in current density values of the two branches (cathodic and anodic) of the polarization curves and consequently the values of i_{corr}.

However, the increase in current density is highly more pronounced in uninhibited than in inhibited media. Indeed, it is worth noting that the values of i_{corr} in the presence of 150 ppm NA1 are always smaller than in its absence. Moreover, no clear trends are observed in E_{corr} values at higher temperatures in the inhibitor-free medium and with NA1. These results reflect the enhancement of both the cathodic hydrogen evolution reaction as well as anodic mild steel dissolution with a temperature rise.

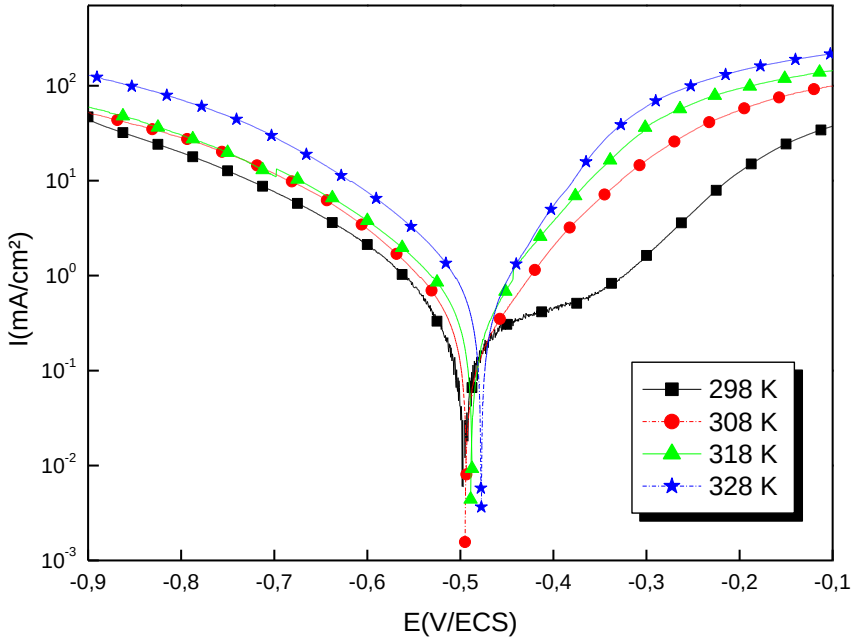

Figure 6. Polarization curves of steel in HCl 1 M at different temperatures.

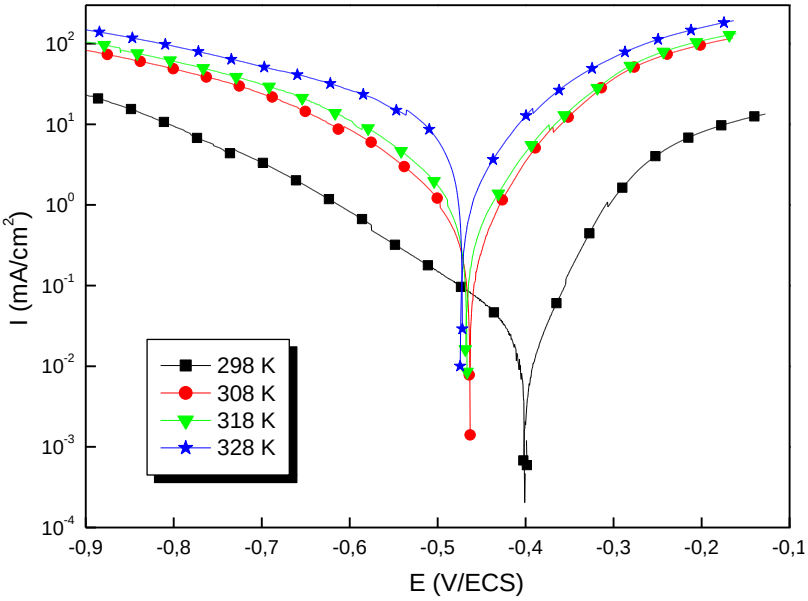

Figure 7. Polarization curves of steel in HCl 1 M with 150 ppm of NA1 at different temperatures.

Table 6. Electrochemical parameters of steel at different temperatures in 1 M HCl without and with NA1.

Compounds	Temperature K	$-E_{corr}$ (mV/ECS)	i_{corr} (μA/cm²)	$-\beta_c$ (mV/dec)	β_a (mV/dec)	E%
Blank	298	498	983	92	104	–
	308	491	1200	184	112	–
	318	475	1450	171	124	–
	328	465	2200	161	118	–
NA1	298	397	102	118	43	89.6
	308	460	150	83	57	87.5
	318	462	203	82	61	86.0
	328	469	340	71	64	84.5

3.5.2. Thermodynamic part

The dependence of the corrosion rate on the temperature can be expressed by the Arrhenius equation:

$$\ln i_{corr} = \ln A - \frac{E_a}{RT} \quad (6)$$

where E_a is the activation energy of corrosion process, R is the universal gas constant, A is the Arrhenius pre-exponential constant and T is the absolute temperature. In addition, the i_{corr} values were calculated in order to determine the activation energy of corrosion E_a, which could give information about the mechanism of adsorption.

In order to assure that the achieved coverage degree is close to the maximal value, *i.e.*, the concentration which gives the best inhibiting efficiency, the Arrhenius plot according to equation (6) is presented in Figure 8 in the absence and in the presence of 150 ppm of NA1. The apparent activation energy values (E_a) for mild steel in 1 M HCl in the absence and in the presence of 150 ppm of NA1 were determined from the slope of $\ln i_{corr}$ *vs.* $1000/T$ plots and shown in Table 7.

Table 7. The values of activation parameter (E_a) for mild steel in 1 M HCl and in the absence and in the presence of 150 ppm of NA1.

	E_a, kJ/mol
Blank	31.51
150 ppm NA1	51.72

As observed in Table 7, the E_a increases in the presence of 150 ppm NA1 in the acid medium. The increase in E_a in the presence of NA1 may be interpreted as physical adsorption. Indeed, a higher energy barrier for the corrosion process in the inhibited solution is associated with physical adsorption or weak chemical bonding between the inhibitor species and the steel surface [39–45].

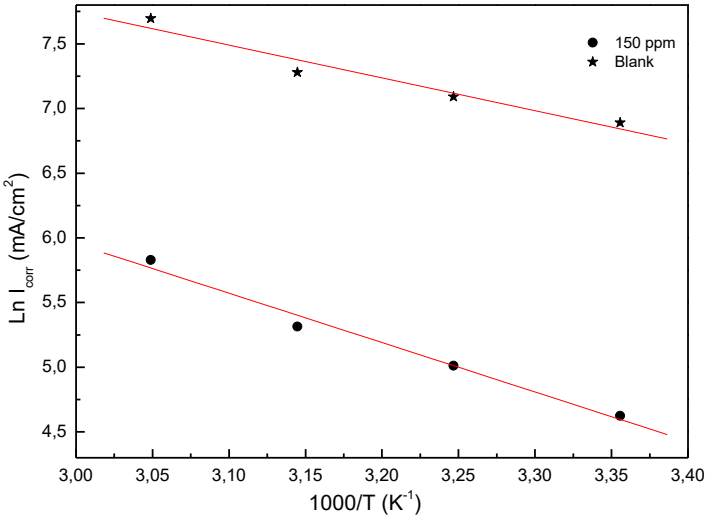

Figure 8. Arrhenius plots of mild steel in 1 M HCl in the absence and in the presence of 150 ppm NA1.

3.6. Effect of the glass composition on the corrosion resistance

The behavior of mild steel in 1 M HCl solution for different compositions of glasses in the system $(0.90–x)Bi_2O_3–xB_2O_3–(0.05V_2O_5–0.05Nb_2O_5)$ namely NA (from NA1 to NA5) at 150 ppm was investigated using the EIS method at room temperature after 1/2 h of immersion at the corrosion potential (Figure 9).

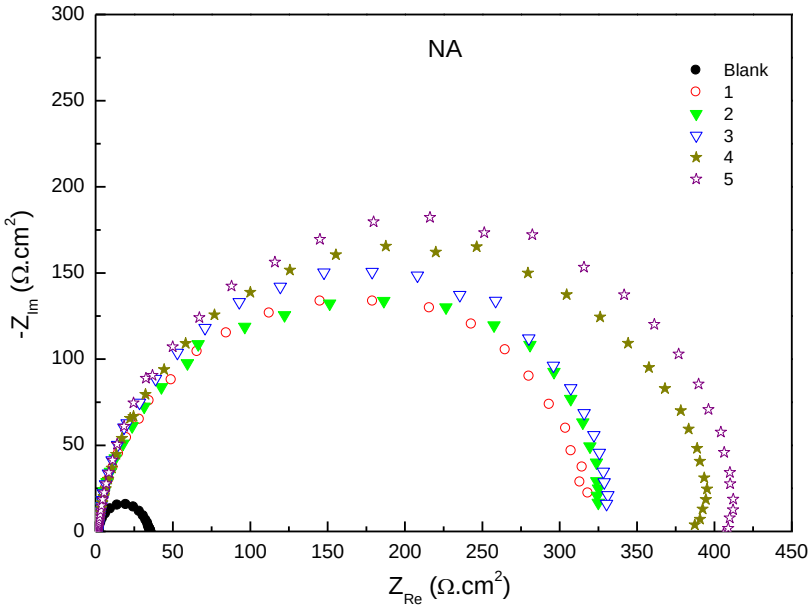

Figure 9. Impedance diagrams at the corrosion potential of steel in HCl 1 M without and with 150 ppm of NA inhibitor.

The results described below can be interpreted in terms of the equivalent circuit of the electrical double layer shown in Figure 9, which was used previously to simulate the iron-

acid interface [46]. The impedance diagrams obtained are not perfect semicircles and this difference was attributed to frequency dispersion [47]. It is apparent from these plots that the impedance response of mild steel in uninhibited 1 M HCl solution changed significantly after addition of each inhibitor. It is higher for a higher content of B_2O_3. The electrochemical parameters derived from the Nyquist plots and inhibition efficiency values are given in Table 8. For all percentages of B_2O_3, the charge transfer resistance increases compared to the blank solution. This change can result from a decrease in local dielectric constant and/or an increase in the thickness of the electrical double layer, suggesting that the inhibitor molecules function by adsorption at the metal–solution interface [48]. In this way the presence of V_2O_5 decrease the resistance of mild steel (axis NA) [49].

Table 8. Electrochemical parameters from the Nyquist plots and values of the inhibition efficiency of steel in 1 M HCl without and with 150 ppm of NA inhibitor.

	R_{ct} ($\Omega \cdot cm^2$)	C_{dl} ($\mu F \cdot cm^{-2}$)	η_{imp} %
Blank	35	298	
NA1	326	58	89.2
NA2	327	57	89.3
NA3	329	53	89.4
NA4	397	46	91.2
NA5	417	41	91.6

3.7. Surface analysis

In this study the surface of the steel was characterized by SEM. The image of mild steel after 6 hours of immersion in HCl 1.0 M solution without NA1 at 298 K was observed. Figure 10(a–b) (SEM/EDX image of (a): Blank immersed at 1 M HCl, (b): 150 ppm of NA1 inhibitor, respectively) shows the SEM images of uninhibited and inhibited mild steel specimens in 1 M HCl immersed for 6 h at the effective concentration of the inhibitor. We observed that MS surface in the absence of NA1 is highly corroded because of the free acid attack without surface protection. However, in the presence of 150 ppm of NA1, the surface morphology is remarkably improved [38, 50]. An increase in the surface morphologies in the presence of NA1 suggests that they adsorb at the metal-electrolyte interfaces and form inhibitive films. We realized EDX analysis in order to identify the different elements present on the mild steel surface. Figure 10 presents the EDX spectra. In the case of the blank solution, we note the formation of iron oxide and the appearance of an oxygen peak emerging from the steel attack in HCl 1.0 M. We note also that in the presence of NA1, a decrease in the carbon and oxygen peaks and the presence of bismuth and phosphor. These observations confirm that the glassy compound decreases steel corrosion by forming a layer, which restricts electrolyte access to the surface of the steel [38].

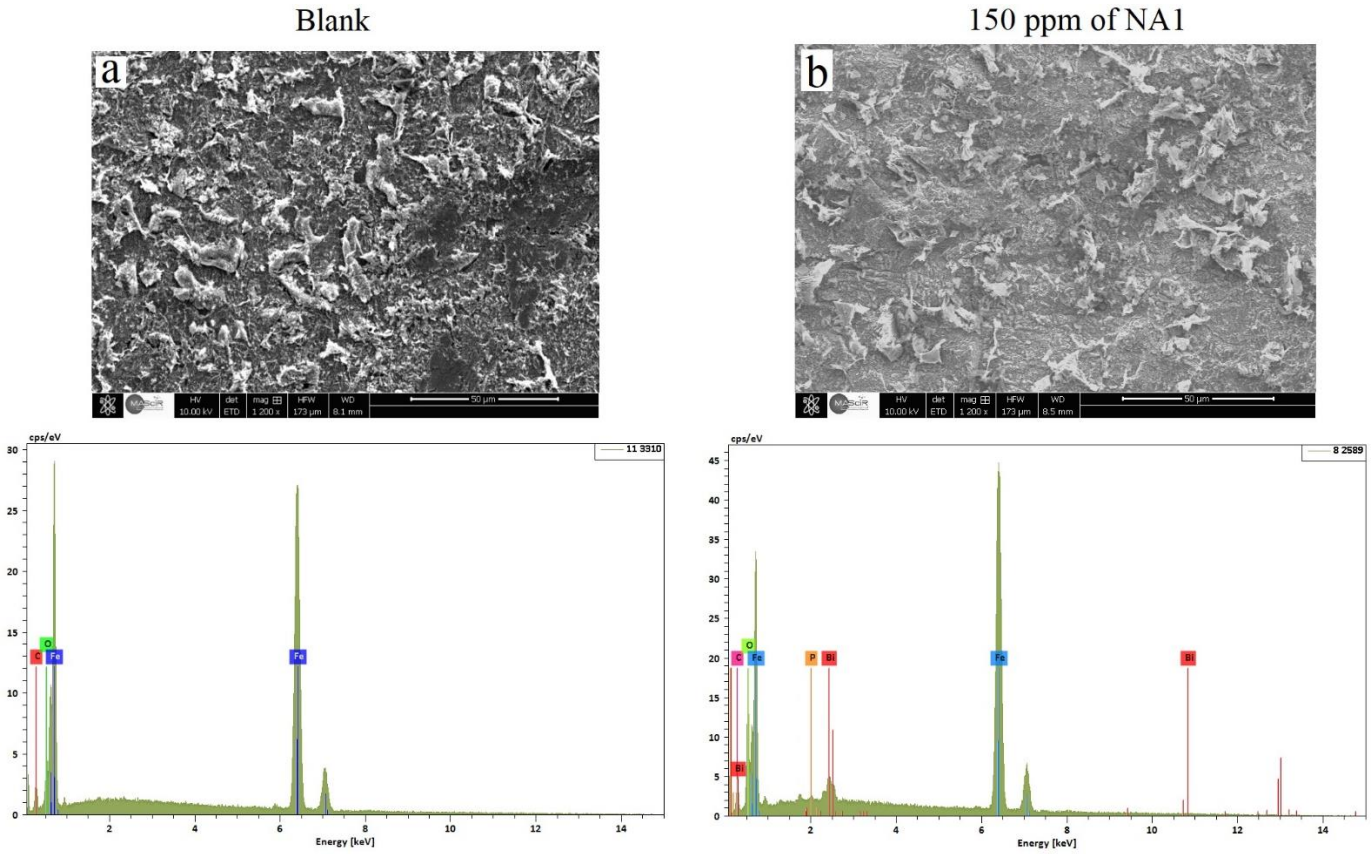

Figure 10. SEM image/EDX of mild steel after 6 h of immersion in 1.0 M HCl solution with 150 ppm of NA1 at 298 K.

4. Conclusion

Glasses of the $(0.90–x)Bi_2O_3–xB_2O_3–(0.05V_2O_5–0.05Nb_2O_5)$ system were prepared, which allowed the delimitation of the vitreous zone. The inhibition of steel corrosion in 1 M HCl acid medium by glasses of the $(0.90–x)Bi_2O_3–xB_2O_3–(0.05V_2O_5–0.05Nb_2O_5)$ system was studied by stationary polarization and electrochemical impedance spectroscopy. The results showed a significant decrease in the corrosion current and an increase in charge transfer resistance when the vitreous compounds were added to the corrosive solution. This inhibition depends on the composition of the vitreous phase. The inhibitory efficiency reaches 89% for NA at a concentration of 150 ppm. The system acts primarily as an anodic inhibitor by forming a stable film on the steel surface. The thermodynamic study showed that this film was formed by physisorption. Moreover, the inhibition efficiency increases with B_2O_3 content reaching a maximum value at 50% of B_2O_3. The presence of V_2O_5 decreases the inhibition efficiency.

References

1. Y.El. Kacimi, R. Touir, M. Galai, R.A. Belakhmima, A. Zarrouk, K. Alaoui, M. Harcharras, H.El Kafssaoui and M. Touhami, Effect of silicon and phosphorus contents in steel on its corrosion inhibition in 5 M HCl solution in the presence of Cetyltrimethylammonium/KI, *J. Mater. Environ. Sci*., 2016, **7**, no. 1, 371–381.
2. L. Larabi, Y. Harek, O. Benali and S. Ghalem, Hydrazide derivatives as corrosion inhibitors for mild steel in 1 M HCl, *Prog. Org. Coat*., 2005, **54**, no. 3, 256–262. doi: 10.1016/j.porgcoat.2005.06.015
3. M. Mihit, K. Laarej, H.A. El Makarim, L. Bazzi, R. Salghi and B. Hammouti, Study of the inhibition of the corrosion of copper and zinc in HNO_3 solution by electrochemical techniqueand quantum chemical calculations, *Arabian J. Chem*., 2010, **3**, no. 1, 55–60. doi: 10.1016/j.arabjc.2009.12.009
4. O. Benali, L. Larabi, S. Merah and Y. Harek, Influence of the methylene blue dye (MBD) on the corrosion inhibition of mild steel in 0.5 M sulphuric acid, part I: weight loss and electrochemical studies, *J. Mater. Environ. Sci*., 2011, **2**, no. 1, 39–48.
5. M. Galai, M. Rbaa, Y.El Kacimi, M. Ouakki, N. Dkhirech, R. Touir, B. Lakhrissi and M. Ebn Touhami, Anti-corrosion Properties of some Triphenylimidazole Substituted Compounds in Corrosion Inhibition of Carbon Steel in 1.0 M Hydrochloric Acid Solution, *Anal. Bioanal. Electrochem*., 2017, **9**, no. 1, 80–101.
6. O. Benali, L. Larabi, S.M. Mekelleche and Y. Harek, Influence of substitution of phenyl group by naphthyl in a diphenyl thiourea molecule on corrosion inhibition of cold-rolled steel in 0.5 M H_2SO_4, *J. Mater. Sci*., 2006, **41**, 7064–7073.
7. S. Merah, L. Larabi, O. Benali and Y. Harek, Synergistic effect of methyl red dye and potassium iodide on inhibition of corrosion of carbon steel in 0.5 M H_2SO_4, *Pigm. Resin Technol*., 2008, **37**, no. 5, 291–298. doi: 10.1108/03699420810901963
8. D.B. Hmamou, R. Salghi, A. Zarrouk, H. Zarrok, B. Hammouti, S.S. Al-Deyab, M. Bouachrine, A. Chakir and M. Zougagh, Alizarin red: an efficient inhibitor of C38 steel corrosion in hydrochloric acid, *Int. J. Electrochem. Sci*., 2012, **7**, 5716–5733.
9. W.D. Robertson, Molybdate and tungstate as corrosion inhibitors and the mechanism of inhibition, *J. Electrochem. Soc*.,1951, **98**, no. 3, 94–100. doi: 10.1149/1.2778118
10. G.H. Cartledge, Passivation and Activation of Iron in the Presence of Molybdate Ions, *Corrosion*,1968, **24**, no. 8, 223–236. doi: 10.5006/0010-9312-24.8.223
11. C. Breslin, G. Treacy and W. Carroll, Studies on the passivation of aluminium in chromate and molybdate solutions, *Corros. Sci*., 1994, **36**, no. 7, 1143–1154. doi: 10.1016/0010-938X(94)90139-2
12. W. Badawy, F. Al-Kharafi and A. El-Azab, Electrochemical behavior and corrosion inhibition of Al, Al-6061 and Al–Cu inneutral aqueous solutions, *Corros. Sci*., 1999, **41**, no. 4, 709–727. doi: 10.1016/S0010-938X(98)00145-0
13. K. Alaoui, Y. El Kacimi, M. Galai, R. Touir, K. Dahmani, A. Harfi and M. Ebn Touhami, Anti-corrosive properties of polyvinyl-alcohol for carbon steel in

hydrochloric acid media: electrochemical and thermodynamic investigation, *J. Mater. Environ. Sci*., 2016, **7**, 2389–2403.
14. K. Dahmani, M. Galai, M. Ouakki, M. Cherkaoui, R. Touir, S. Erkan, S. Kaya and B.El Ibrahimi, Quantum chemical and molecular dynamic simulation studies for the identification of the extracted cinnamon essential oil constituent responsible for copper corrosion inhibition in acidified 3.0 wt% NaCl medium, *Inorg. Chem. Commun*., 2021, **124**, 108409. doi: 10.1016/j.inoche.2020.108409
15. M. Stern and A.L. Geary, Electrochemical Polarization: A Theoretical Analysis of the Shape of Polarization Curves, *J. Electrochem. Soc*., 1957, **104**, 56–63. doi: 10.1149/1.2428496
16. B.A. Bouckamp, *Users manual equivalent circuit*, ver. 4.51, Faculty of Chem. Tech., Universidad of Twente, The Netherlands, 1993.
17. T. Guedira, Contributionà l'identification des isothermes vers 820°C des ternaires MO_X–Bi_2O_3–P_2O_5 (*M*=Li, Ca, Ba, B, Sb, Zr, Sn, Nb, Ta). Etude des phases, sillenite, fluorine et vitreuses, Thèse de Doctorat D'Etat ES-Sciences. Université Ibn Tofail, Faculté des sciences, kenitra, 2003.
18. M. Belfaquir, T. Guedira, S.D. Elyoubi and J.L. Rehspringe, Synthèse et caractérisation des phases du système ternaire Bi_2O_3–P_2O_5–B_2O_3, *Ann. Chim. Sciences Matériaux*., 2005, **30**, no. 1, 27–35.
19. M. Belfaquir, T. Guedira, S.D. Elyoubi and J.L. Rehspringer, Etude structurale des verres borate du système ternaire Bi_2O_3–P_2O_5–B_2O_3, *Sciences Lib Editions Mersenne*, 2013, **5**, 130302.
20. J. Zarzycki, *Les verres et l'état vitreux*, ED, Masson, Paris, 1982.
21. W.H. Zachariasen, The atomic arrangement in glass, *J. Am. Chem. Soc*., 1932, **54**, no. 10, 3841–3851. doi: 10.1021/JA01349A006
22. K.H. Sun, Fundamental condition of glass formation, *J. Am. Chem. Soc*., 1947, **30**, no. 9, 277–281. doi: 10.1111/J.1151-2916.1947.TB19654.X
23. V.M. Goldschmidt, Über das krystallochemische und geochemische Verhalten des Germaniums, *NaturwissKlasse*, 1926, **14**, 295–297.
24. U.H. Zachariasen, Natural and Synthetic Rubber. VIII. Products of the Destructive Distillation of Sodium Rubber, *J. Am. chem. Soc*., 1932, **54**, no. 1, 381–386. doi: 10.1021/JA01340A058
25. H.El Boulifi, M. Ouakki, H. Barebita, T. Guedira and M. Cherkaoui, Assessing the corrosion inhibition performance of two borate-based glasses for mild steel in hydrochloric acid, *Mater. Today: Proc*., 2021, **37**, no. 3, 3967–3972. doi: 10.1016/j.matpr.2020.09.658
26. A.J. Semkal, The surface tension and structure of silicate slags, *J. Soc. Glass Technol*., 1951, **35**, 411.
27. A. Osaka, M. Ikeda, H. Ohbayashi and K. Takahashi, Network structure of borophosphate glasses (Part 2) Raman spectra of potassium borophosphate glasses, *J. Ceram. Soc. Jpn*., 1988, **96**, 521–524.

28. L. Pauling, *The nature of the chemical bond*, 3rd ed., Cornell Ithaca, 1960, 242.
29. M.R. Ali, C.M. Mustafa and M. Habib, Effect of molybdate, nitrite and zinc ions on the corrosion inhibition of mild steel inaqueous chloride media containing cupric ions, *J. Sci. Res*., 2009, **1**, no. 1, 82–91. doi: 10.3329/JSR.V1I1.1053
30. S. Ferraa, M. Ouakki, H. Barebita, A. Nimour, M. Cherkaoui and T. Guedira, Corrosion inhibition potentials of some phosphovanadate-based glasses on mild steel in 1 M HCl, *Inorg. Chem. Commun*., 2021, **132**, 108806.
31. T. Takahashi, H. Iwahara and Y. Nagai, High oxide ion conduction in sintered Bi_2O_3 containing SrO, CaO or La_2O_3, *J. Appl. Electrochem*., 1972, **2**, 97–104. doi: 10.1007/BF00609125
32. L. Pauling, *The nature of the chemical bond .3ed*, Cornell Ithaca, 1960.
33. E.S. Ferreira, C. Giancomlli, F.C. Giacomlli and A. Spinelli, Evaluation of the inhibitor effect of L-ascorbic acid on the corrosion of mild steel, *Mater. Chem. Phys*., 2004, **83**, no. 1, 129–134. doi: 10.1016/j.matchemphys.2003.09.020
34. N. Dkhireche, M. Galai, Y.El Kacimi, M. Rbaa, M. Ouakki, B. Lakhrissi and M. Ebn Touhami, New quinoline derivatives as sulfuric acid inhibitor's for mild steel, *Anal. Bioanal. Electrochem*., 2018, **10**, no. 1, 111–135.
35. M. Rbaa, M. Ouakki, M. Galai, A. Berisha, B. Lakhrissi, C. Jama, I. Warad and A. Zarrouk, Simple preparation and characterization of novel 8-Hydroxyquinoline derivatives as effective acid corrosion inhibitor for mild steel: Experimental and theoretical studies, *Colloids Surf., A*, 2020, **602**, 125094. doi: 10.1016/j.colsurfa.2020.125094
36. M. Ouakki, M. Galai, M. Rbaa, A.S. Abousalem, B. Lakhrissi, M.Ebn Touhami and M. Cherkaoui, Electrochemical, thermodynamic and theoretical studies of some imidazole derivatives compounds as acid corrosion inhibitors for mild steel, *J. Mol. Liq*., 2020, **319**, 114063. doi: 10.1016/j.molliq.2020.114063
37. M. Galai, M. Rbaa, H. Serrar, M. Ouakki, A. Ech-chebab, A.S. Abousalem, E. Ech-chihbi, K. Dahmani, S. Boukhris, A. Zarrouk and M. Ebn Touhami, S-Thiazine as effective inhibitor of mild steel corrosion in HCl solution: Synthesis, experimental, theoretical and surface assessment, *Colloids Surf., A*, 2021, **613**, 126127. doi: 10.1016/j.colsurfa.2020.126127
38. G. Ghenimi, M. Ouakki, H. Barebita, A.El Fazazi, T. Guedira and M. Cherkaoui, New Vitreous Phase as Mild Steel Inhibitors in Hydrochloric Acid, *Anal. Bioanal. Electrochem*., 2020, **12**, no. 1, 1–20.
39. E. Ech-chihbi, A. Nahlé, R. Salim, F. Benhiba, A. Moussaif, F. El-Hajjaji, H. Oudda, A. Guenbour, M. Taleb, I. Warad and A. Zarrouk, Computational, MD simulation, SEM/EDX and experimental studies for understanding adsorption of benzimidazole derivatives as corrosion inhibitors in 1.0 M HCl solution, *J. Alloys Compd*., 2020, **844**, 155842. doi: 10.1016/j.jallcom.2020.155842

40. M. Rbaa, M. Galai, M.E.L. Faydy, Y.El Kacimi, M. Ebn Touhami, A. Zarrouk and B. Lakhrissi, Synthesis and Characterization of New Benzimidazoles Derivatives of 8-hydroxyquinoline as a Corrosion Inhibitor for Mild Steel in 1.0 M Hydrochloric Acid Medium, *J. Mater. Environ. Sci*., 2017, **8**, no. 7, 3529.
41. M. Yadav, S. Kumar, R.R. Sinha and D. Behera, Experimental and quantum chemical studies on the corrosion inhibition performance of benzimidazole derivatives for mild steel in HCl, *Ind. Eng. Chem. Res*., 2013, **52**, no. 19, 6318–6328. doi: 10.1021/IE400099Q
42. M. Ouakki, M. Galai, M. Rbaa, A.S. Abousalem, B. Lakhrissi, E.H. Rifi and M. Cherkaoui, Quantum chemical and experimental evaluation of the inhibitory action of two imidazole derivatives on mild steel corrosion in sulphuric acid medium, *Heliyon*, 2019, **5**, no. 11, e02759. doi: 10.1016/j.heliyon.2019.e02759
43. M. Ouakki, M. Galai, M. Cherkaoui, EH. Rifi and Z. Hatim, Inorganic Compound (Apatite doped by Mg and Na) as a Corrosion Inhibitor for Mild Steel in Phosphoric Acidic Medium, *Anal. Bioanal. Electrochem*., 2018, **10**, no. 7, 943–960.
44. M. Yadav, S. Kumar, N. Tiwari, I. Bahadur and EE. Ebenso, Experimental and quantum chemical studies of synthesized triazine derivatives as an efficient corrosion inhibitor for N80 steel in acidic medium, *J. Mol. Liq*., 2015, **212**, 151–167. doi: 10.1016/j.molliq.2015.09.019
45. K. Alaoui, Y.El Kacimi, M. Galai, K. Dahmani, A.E. El Harfi, R. Touir and M. Ebn Touhami, Poly (1-phenylethene): as a novel corrosion inhibitor for carbon steel/hydrochloric acid interface, *Anal. Bioanal. Electrochem*., 2016, **8**, 830–847.
46. M. Cissé, M. Abouchane, T. Anik, K. Himm, R.A. Belakhmima, M. Ebn Touhami, R. Touir and A. Amiar, Corrosion Resistance of Electroless Ni-Cu-P Ternary Alloy Coatings in Acidic and Neutral Corrosive Mediums, *Int. J. Corros*., 2010, **2010**. Doi: 10.1155/2010/246908
47. M. Galai, M. Rbaa, M. Ouakki, A.S. Abousalem, E. Ech-chihbi, K. Dahmani, N. Dkhireche, B. Lakhrissi and M. Ebn Touhami, Chemically functionalized of 8-hydroxyquinoline derivatives as efficient corrosion inhibition for steel in 1.0 M HCl solution: Experimental and theoretical studies, *Surf. Interfaces*, 2020, **21**, 100695. doi: 10.1016/j.surfin.2020.100695
48. R. Touir, N. Dkhireche, M. Ebn Touhami, M. Sfaira, O. Senhaji, J.J. Robin, B. Boutevin and M. Cherkaoui, Study of phosphonate addition and hydrodynamic conditions on ordinary steel corrosion inhibition in simulated cooling water, *Mater. Chem. Phys*., 2010, **122**, no. 1, 1–9. doi: 10.1016/j.matchemphys.2010.02.063
49. A. Majjane, D. Rair, A. Chahine, M. Et-tabirou, M. EbnTouhami and R. Touir, Preparation and characterization of a new glass system inhibitor for mild steel corrosion in hydrochloric solution, *Corros. Sci*., 2012, **60**, 98–103. doi: 10.1016/j.corsci.2012.04.006

50. M. Ouakki, M. Galai Z. Benzekri, Ch. Verma, E. Ech-chihbi, S. Kaya, S. Boukhris, E.E. Ebensog, M. EbnTouhami and M. Cherkaoui, Insights into corrosion inhibition mechanism of mild steel in 1 M HCl solution by quinoxaline derivatives: electrochemical, SEM/EDAX, UV-visible, FT-IR and theoretical approaches, *Colloids Surf., A*, 2020, **611**, 125810. doi:10.1016/j.colsurfa.2020.125810

♦ ♦ ♦